Temporal Characterization of a Self-Modulated Laser Wakefield

S. P. Le Blanc,[1,2] M. C. Downer,[1,2] R. Wagner,[1] S.-Y. Chen,[1] A. Maksimchuk,[1] G. Mourou,[1] and D. Umstadter[1]

[1]Center for Ultrafast Optical Science, University of Michigan, Ann Arbor, Michigan 48109

[2]Department of Physics, The University of Texas at Austin, Austin, Texas 78712

(Received 9 September 1996)

The temporal envelope of plasma density oscillations in the wake of an intense ($I \sim 4 \times 10^{18}$ W/cm^2, $\lambda = 1$ μm) laser pulse (400 fs) is measured using forward Thomson scattering from a copropagating, frequency-doubled probe pulse. The wakefield oscillations in a fully ionized helium plasma ($n_e = 3 \times 10^{19}$ cm^{-3}) are observed to reach maximum amplitude ($\delta n_e/n_e \sim 0.1$) 300 fs after the pump pulse. The wakefield growth (3.5 ps^{-1}) and decay (1.9 ps^{-1}) rates are consistent with the forward Raman scattering instability and Landau damping, respectively. [S0031-9007(96)02024-8]

PACS numbers: 52.40.Nk, 52.35.Mw

Because electrostatic fields in a relativistic plasma wave ($E \gtrsim 100$ GV/m) can exceed by 3 orders of magnitude those in conventional rf linacs, plasma based accelerators can provide a compact source for high energy electron pulses [1]. Of the several methods for driving large amplitude plasma waves, the laser wakefield accelerator (LWFA) [1] and its variant, the self-modulated LWFA [1–7], have recently received considerable attention because of the reduction in size of terawatt class laser systems [8]. In the LWFA, the amplitude $\alpha = \delta n_e/n_e$ of the plasma wave can be resonantly excited by the ponderomotive force of the laser pulse if the laser pulse duration is approximately half of the plasma wave period $\tau_p = 2\pi/\omega_p$, where $\omega_p = \sqrt{4\pi e^2 n_e/m_e}$ is the electron plasma frequency and n_e is the plasma density.

For the self-modulated LWFA, the plasma density is chosen to be much larger than for the standard LWFA so that the forward Raman scattering (FRS) instability can grow. The FRS instability is the conversion of an electromagnetic wave (ω_0, k_0) into a plasma wave (ω_p, k_p) and Stokes ($\omega_0 - \omega_p, k_0 - k_p$) and anti-Stokes ($\omega_0 + \omega_p, k_0 + k_p$) electromagnetic sidebands [9]. Electron density perturbations in the plasma cause local variations in the group velocity $v_g = c(1 - \omega_p^2/w_0^2)^{1/2}$ of the laser pulse. As a result, light that propagates near a density maximum (minimum) will slow down (speed up). Eventually, the light is bunched to positions where $\delta n_e = 0$. Because the plasma density perturbation and the bunching of the light are $\pi/2$ out of phase, the ponderomotive force of the bunched light will reinforce the original density perturbation. Since the maximum longitudinal electric field E_z scales as $E_z \propto \alpha \sqrt{n_e}$, the self-modulated wakefield can produce a much larger accelerating field than the standard LWFA. In this Letter, we report time resolved measurements of the amplitude of the self-modulated laser wakefield obtained using forward Thomson scattering from a copropagating, frequency-doubled probe pulse [10]. In addition to measuring the growth and decay rate of the wakefield, we report that the onset of FRS is consistent with a plasma density perturbation driven by the ionization front of the laser pulse. These observations are

important for testing recently developed 2D particle-in-cell simulations of laser plasma interactions [11–13] and for the design of future plasma based accelerators.

In the present experiments, a hybrid Ti:sapphire–Nd:glass laser system capable of delivering 3 J, 400 fs laser pulses was used to drive the self-modulated LWFA. The 43 mm diameter beam was focused by an $f/4$ off-axis parabolic mirror to a spot size (e^{-2} intensity) of $r_0 = 8.9$ μm, giving a maximum vacuum intensity of $I = 6 \times 10^{18}$ W/cm^2 ($a_0 = 2.2$). The laser was focused onto a supersonic helium gas jet whose neutral density varied linearly with backing pressure [7]. To probe the lifetime of the plasma wave, a small portion (20%) of the infrared laser pulse was split off, frequency doubled in a 4 mm type I potassium dihydrogen phosphate (KDP) crystal, and then made to copropagate with the infrared pump pulse. The temporal overlap between the IR pump pulse and orthogonally polarized green probe pulse was measured with a resolution of ±100 fs by frequency domain interferometry. The probe pulse had a maximum energy of 15 mJ and could be focused to a spot size of 6.4 μm by the harmonically coated parabolic mirror. Forward scattered light from the probe pulse was collected on axis, passed through a polarizer to suppress scattered pump light, and measured with a prism spectrometer which has a resolution of $\lambda/\Delta\lambda = 600$ at $\lambda = 1.053$ μm.

When the peak power of the IR pump pulse ($P \gtrsim 1$ TW) is near the critical power for relativistic self-focusing $P_c = 17(\omega_0^2/\omega_p^2)$ GW, the forward scattered light from the pump pulse shows the appearance of three anti-Stokes Raman shifted sidebands separated by the plasma frequency ($\omega_p \sim 3 \times 10^{14}$ s^{-1}) [7]. Numerical simulations indicate that the appearance of multiple sidebands is clear evidence of FRS. From the relative amplitude of the Raman satellites, the plasma wave amplitude is estimated to be $\delta n/n = 0.08-0.4$, depending on the pump power and plasma density [7]. Under these conditions, a collimated beam of 2 MeV electrons is emitted in the laser propagation direction [7].

In one dimension, the spatiotemporal growth rate for the FRS instability starting from a uniform noise source δn_s

is given by [11]

$$\delta n = \begin{cases} \delta n_s \cosh(\gamma_0 \tau), & \psi \geq \tau c, \\ \delta n_s \sum (\frac{\psi/c}{\tau - \psi/c})^n I_{2n}(2\gamma_0 \sqrt{(\tau - \psi/c)\psi/c}), & \tau c \geq \psi, \end{cases} \tag{1}$$

where I_{2n} is the modified Bessel function of the first kind, ψ is the distance from the leading edge of the pulse, τ is the propagation time, a_0 is the normalized vector potential of the laser, and $\gamma_0 = a_0 \omega_p^2 / \omega_0 \sqrt{8} (1 + a_0^2/2)^{1/2}$ is the temporal growth rate. Because the laser pulse changes shape as the instability grows, FRS for relativistic intensity laser pulses is a highly nonlinear process.

When the green probe pulse propagates through the plasma, collective Thomson scattering from the relativistic plasma wave causes multiple sidebands to appear in the spectrum of the forward scattered probe light. For $P = 3$ TW and a backing pressure of 100 psi, Fig. 1 shows the appearance of first and second order Thomson scattered satellites which are separated by the plasma frequency $\omega_p = 2.7 \times 10^{14}$ s^{-1}. The amplitude of the plasma wave can be determined from both the absolute and relative scattering efficiency of the Thomson sidebands. For collective Thomson scattering, the absolute scattering efficiency is given by [14]

$$\frac{P_s}{P_0} = \frac{1}{4} (\delta n_e)^2 r_0^2 \lambda_0^2 L^2 \frac{\sin^2(\Delta k L)}{(\Delta k L)^2}, \tag{2}$$

where r_0 is the classical electron radius, λ_0 is the wavelength of the incident light, L is the interaction length, $\Delta k = k_0 - k_s \pm k_p$ is the wave vector mismatch, $k_p = \omega_p/v_p$, and the phase velocity v_p of the plasma wave is equal to v_g of the pump pulse. For direct forward scatter of the first anti-Stokes sideband ($\Delta k = 8 \times 10^3$ m^{-1}) and L equal to the confocal beam parameter ($L = 430$ μm), the phase mismatch factor $F = \sin^2(\Delta k L)/(\Delta k L)^2 = 0.02$ and the amplitude of the plasma wave is determined to be $\alpha = 0.08$. Similarly, from the first Stokes line, $\alpha = 0.06$. Applying the same analysis to the second order satellites, the amplitude of the second harmonic of the plasma wave is $\delta n_2/n = 0.01$.
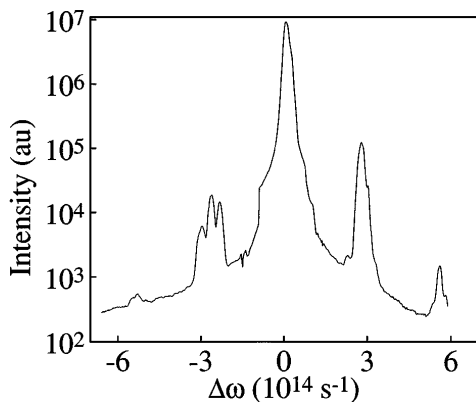

FIG. 1. Spectrum of the Thomson scattered probe light for a helium backing pressure of 100 psi, $P_{pump} = 3$ TW, and $\Delta t = 0$.

From harmonic wave analysis [15], the fundamental amplitude of the plasma wave is related to its second harmonic by $\alpha \sim (\delta n_2/n)^{1/2}$, or $\alpha = 0.1$ for the present conditions at 100 psi backing pressure. Using harmonic analysis and Eq. (2), the relative amplitude of the first and second order Thomson satellites can be used to determine α without specifying L: $\alpha \sim (P_2/P_1)^{1/2}$, or $\alpha = 0.1$. Thus, the absolute and relative scattering efficiencies yield plasma wave amplitudes that are in good agreement. For a Gaussian laser focus, the peak amplitude is estimated to be $\alpha_p = 0.2$.

By measuring Thomson scattering from the probe pulse as a function of the delay between the pump and probe, the temporal envelope of the wakefield oscillations can be recorded. Figure 2(a) shows the change in the spectrum of the probe pulse as the delay (Δt) between a 600 mJ (1.5 TW) pump and a 15 mJ probe pulse is varied from -1 to 3 ps. Only the first order Thomson scattered satellites are shown. When the Thomson scattered satellites first become observable ($\Delta t \sim -700$ fs), their frequency shift is $\Delta \omega = 3 \times 10^{14}$ s^{-1}. The frequency shift then increases gradually and becomes fixed at $\Delta \omega = 3.3 \times 10^{14}$ s^{-1} for $\Delta t \geq 0$, because it takes a finite time for the helium to become fully ionized. Simultaneously, a blueshifted wing appears on the green probe pulse because of the rapid increase in the electron density [16]. This temporal position of the ionization front is consistent with a calculation of field ionization of helium for our pump pulse parameters.

At most delay times, the amplitude of the anti-Stokes satellite is larger than that of the Stokes due to more favorable phase matching of the anti-Stokes for direct forward scatter. Using the scattering efficiencies of the Stokes and anti-Stokes sidebands and Eq. (2), Fig. 2(b) shows the plasma wave amplitude as a function of the probe delay time. The plasma wave is measured to have a peak amplitude $\alpha = 0.1$, which corresponds to a maximum longitudinal field of $E_z = 56$ GV/m for a cold, nonrelativistic fluid. Under the current tight focusing conditions, the maximum radial electric field is $E_r = 2E_z/k_p r_0 = 0.2E_z$. Large radial fields can give rise to defocusing of the accelerated electron beam. Figure 2(b) shows that the wakefield amplitude maximizes at the end of the pump pulse ($\Delta t = 300 \pm 100$ fs) and lasts for approximately 2 ps longer. The leading edge of the wakefield rises sharply due to the exponential growth rate of FRS. Note that the probe pulse duration ($\sim$300 fs) is much longer than the plasma period ($\tau_p = 21$ fs for $n_e = 3 \times 10^{19}$ cm^{-3}). Therefore, we do not resolve individual wakefield oscillations [17].

As shown in Fig. 2(b), the onset of the plasma wave occurs $\sim$1 ps before the peak of the pump pulse. This observation is contrary to recent 2D simulations which show the plasma wave growing closer to the peak of the pulse [11,13]. In the simulations, the onset of FRS occurs when the leading edge of the pulse is steepened by backward Raman scattering and pump depletion. In
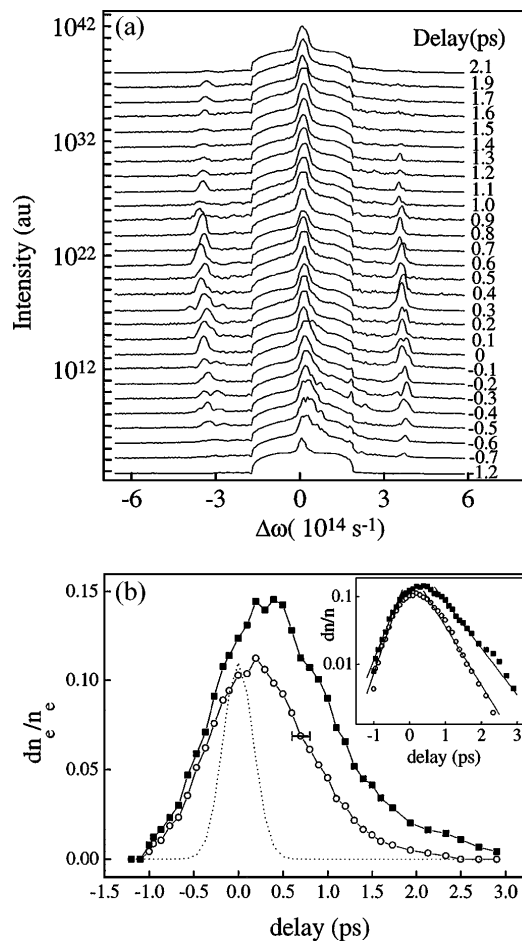
FIG. 2. (a) Forward scattered probe spectra at a helium backing pressure of 180 psi as a function of the delay between the 1.5 TW pump. (b) Plasma wave amplitude determined from the scattering efficiency of the Stokes (filled squares) and anti-Stokes (open circles) satellites as a function of delay. The dotted line indicates the 400 fs pump pulse. A representative horizontal error bar is shown, and the inset shows the exponential fits for the wakefield growth and decay.

the present experiments, FRS starts near the position of the ionization front. The ponderomotive force from an ionization front can create a large amplitude noise source to seed FRS [18]. The ionization front travels at the phase velocity of the plasma wave and creates a noise source that scales as $\delta n_{si}/n \sim a_0^2(\psi_i)/4$, where ψ_i is the position in the pulse where the ionization threshold occurs [19]. For single and double ionization of helium, $\delta n_{si}/n = 10^{-4}$ and 10^{-3}, respectively, which is larger than the noise source due to intensity gradients of the laser pulse $(\delta n_s/n \sim 10^{-6})$ [11]. Consequently, future numerical simulations should include ionization effects.

From the measurements in Fig. 2(b), the wakefield growth and decay rates can be determined. Fitting an exponential to the growth of the plasma wave, the deconvolved growth rate is determined to be 3.5 ± 0.3 ps^{-1} from the anti-Stokes Thomson signal, and 3.3 ± 0.3 ps^{-1} from the Stokes signal. For the current experimental parameters $(\omega_p = 3.3 \times 10^{14}$ s^{-1}, $a_0 = 1)$, the FRS

temporal growth rate $(\gamma_0 = 18$ ps$^{-1})$ overestimates the wakefield growth rate if the peak intensity of the laser pulse is substituted in the expression for γ_0, since the theoretical derivation for γ_0 assumes a constant amplitude pulse. In reality, exponential growth actually takes place during the leading edge of the pulse where $a_0 \ll 1$. For the value of a_0 that is 400 fs before the pump pulse maximum, $\gamma_0 = 8$ ps^{-1}. Since the Rayleigh time $\tau_r = z_r/c$ is longer than the pulse width ψ/c in Eq. (1), the growth of FRS is approximately given by $\delta n = \delta n_s I_0(2\gamma_0\sqrt{\psi\tau/c})$. Evaluation of the Bessel function gives a rise time of 9 ps^{-1} when a_0 is allowed to follow the temporal pulse shape and the interaction length is equal to $2z_r$. A number of factors can cause the measured growth rate to be slightly lower than the calculated growth of four wave resonant FRS. Because FRS is a convective instability, the actual growth rate changes at each delay time (or position ψ). Furthermore, FRS evolves into different regimes—four wave nonresonant, three wave, and self-modulation—as time progresses, each with its own growth rate [19]. For example, the ratio for 1D growth of FRS (Γ_{1D}) to that for 3D self-modulation (Γ_{3D}) is given by $\Gamma_{1D}/\Gamma_{3D} = (k_p^2 r_0^2/2k_0^2)^{1/3}$ [5,20,21]. In the present work, this ratio is unity, so 3D instabilities will compete with 1D FRS. Since the plasma wavelength $(\lambda_p \sim 6$ μm$)$ is comparable to r_0, the plasma wave is near the 3D limit where it has been shown that 1D FRS cannot be resonantly driven because of the complicated three dimensional shape of the plasma wave [11–13].

To further investigate the growth of the wakefield, Thomson scattering was measured as a function of the gas jet backing pressure and the peak power of the pump pulse. Figure 3(a) shows variation in the Thomson spectra for a fixed laser power $(P = 3$ TW$)$ as the helium backing pressure varies from 30 to 180 psi. As expected, the frequency separation between the satellites, given by ω_p, increases as the square root of the backing pressure. For 3 TW pump power, the first anti-Stokes Thomson satellite appears for a backing pressure of 40 psi. From the measured frequency shift of the satellite, the critical power for self-focusing at this backing pressure is $P_c = 1.4$ TW, and thus $P/P_c = 2.1$ and $\gamma_0 = 9$ ps^{-1}. In a similar pressure scan conducted at $P = 1.7$ TW, the first Thomson satellite appeared at a backing pressure of 80 psi where $P/P_c = 1.9$ and $\gamma_0 = 10$ ps^{-1}. As the peak power of the pump pulse increases, Fig. 3(b) shows the change in the Thomson spectra for a fixed backing pressure (180 psi) and at a fixed delay time $(\Delta t = 0)$. The first Thomson scattered satellite appears at $P = 0.78$ TW, or where $P/P_c = 1.7$ and $\gamma_0 = 14$ ps^{-1}. At the threshold for Thomson scattering, the ratio P/P_c decreases as the backing pressure (and hence electron density) increases. This trend is evident from Eq. (1) which indicates that the threshold for FRS depends on ω_p/ω_0 and P/P_c [9]. For both the pressure and power scan in Fig. 3, $\gamma_0 \sim 10$ ps^{-1} even though P/P_c and the backing pressures are different at threshold. The growth rate of the plasma wave
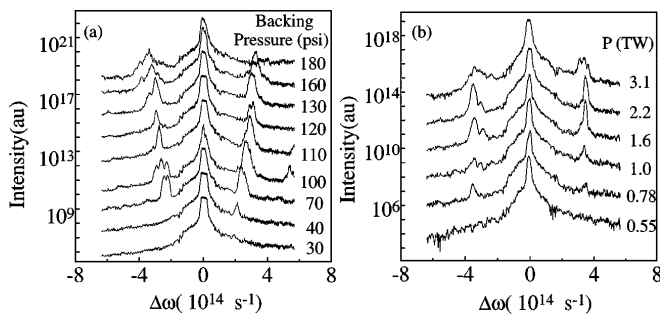
FIG. 3. (a) Pressure dependence of the Thomson scattered probe light for $P = 3$ TW and $\Delta t = 0$. (b) Variation in Thomson scattering with pump pulse power for a fixed backing pressure of 180 psi and $\Delta t = 0$.

as determined by the FRS threshold measurements is in reasonable agreement with the rate obtained from the delay scan in Fig. 2. These observations are also in agreement with those of Ref. [7] which showed that Raman satellites from the pump pulse first appear at $P/P_c = 0.5$ and $\gamma_0 = 6$ ps^{-1} for a helium backing pressure of 150 psi. This indicates that our experiment is in the multidimensional regime of self-modulation [20,21], as distinguished from previous experiments [4–6] which were interpreted within the context of 1D FRS.

The decay of the wakefield is caused by the conversion of collective plasma wave energy into particle energy. In Fig. 2(b), the exponential decay rate of the wakefield is 1.6 ± 0.1 ps^{-1} and 1.9 ± 0.2 ps^{-1} as determined from the Stokes and anti-Stokes Thomson signals, respectively. If the observed damping of the wakefield is due to "beam loading," then the energy in the plasma wave should be transferred to the accelerated electrons. The energy of the plasma wave is approximately given by $W_{\mathrm{wave}} = \epsilon_0 E_z^2 AL/2$, where $A = \pi r_0^2$ and $L = 2z_r$. For $\alpha = 0.1$, $W_{\mathrm{wave}} = 1.6$ mJ. Since this compares well to the energy of 10^9 electrons being accelerated to 2 MeV, or $W_{\mathrm{beam}} = 1$ mJ, it is likely that beam loading and particle acceleration contribute to wakefield decay. The maximum number of electrons N_m that can be accelerated is approximately given by the number required for an electron bunch generated wakefield to cancel the laser induced wakefield. For a short electron bunch, $N_m = 5 \times 10^5 \alpha A \sqrt{(n_o)}$, where n_0 is the electron density in cm^{-3} and A is the cross sectional area of the beam in cm^2 [22]. Under the present conditions, $N_m = 10^9$, which agrees with the total measured value [7]. Since N_m is actually distributed over many particle bunches, the wakefield damps over many oscillation periods.

A complementary way of discussing beam loading is by the concept of Landau damping of trapped electrons. Such trapped electrons come from hot electrons generated by Raman back- and sidescatter, and above threshold ionization (ATI). For $a_0 = 1$, ATI plasma heating is estimated to yield a plasma with $T_e \sim 80$ keV [23], while Raman back- and sidescattering generate hot electrons with $T_e \sim 4$ keV [24] and $T_e \gtrsim 10$ keV [25], respectively.

Since the damping of the plasma wave is dominated by the acceleration of trapped electrons, the rate of decrease of W_{wave} must be equal and opposite to the rate of increase of W_{beam}. From linear theory [26], the Landau damping rate for trapped particles is approximately equal to $\gamma_L = L_d/c$, where L_d is the dephasing length. Under the present conditions, $\gamma_L = 2$ ps^{-1}, which is consistent with the measured wakefield decay rate of 1.9 ps^{-1}. Thus, the wakefield decays at the rate that trapped particles dephase with the plasma wave.

In summary, the rise time of the self-modulated wakefield is in agreement with the growth of the FRS instability, and the decay is consistent with beam loading of the plasma wave. The onset of FRS is coincident with an ionization front induced wakefield, and the detection of a large amplitude plasma wave occurs near the critical power for relativistic self-focusing.

[1] T. Tajima and J. Dawson, Phys. Rev. Lett. **43**, 267 (1979).
[2] C. Joshi *et al.,* Phys. Rev. Lett. **47**, 1285 (1981).
[3] P. Sprangle *et al.,* Phys. Rev. Lett. **69**, 2200 (1992); T. M. Antonsen and P. Mora, Phys. Rev. Lett. **69**, 2204 (1992); N. E. Andreev *et al.,* JETP Lett. **55**, 571 (1992).
[4] C. A. Coverdale *et al.,* Phys. Rev. Lett. **74**, 4659 (1995).
[5] K. Nakajima *et al.,* Phys. Rev. Lett. **74**, 4428 (1995).
[6] A. Modena *et al.,* Nature (London) **377**, 606 (1995).
[7] D. Umstadter *et al.,* Science **273**, 472 (1996).
[8] P. Maine *et al.,* IEEE J. Quantum Electron. **24**, 398 (1988).
[9] W. B. Mori *et al.,* Phys. Rev. Lett. **72**, 1482 (1994).
[10] A. Ting *et al.,* this issue, Phys. Rev. Lett. **77**, 5377 (1996).
[11] C. D. Decker *et al.,* IEEE Trans. Plasma Sci. **24**, 379 (1996); C. D. Decker *et al.,* Phys. Rev. E **50**, 3338 (1994).
[12] S. V. Bulanov *et al.,* Phys. Rev. Lett. **74**, 710 (1995).
[13] K.-C. Tzeng *et al.,* Phys. Rev. Lett. **76**, 3332 (1996).
[14] R. E. Slusher and C. M. Surko, Phys. Fluids **23**, 472 (1980).
[15] D. Umstadter *et al.,* Phys. Rev. Lett. **59**, 292 (1987).
[16] W. M. Wood *et al.,* Phys. Rev. Lett. **67**, 3523 (1991).
[17] C. W. Siders *et al.,* Phys. Rev. Lett. **76**, 3570 (1996); J. R. Marques *et al., ibid.* **76**, 3566 (1996).
[18] W. B. Mori and T. Katsouleas, Phys. Rev. Lett. **69**, 3495 (1992).
[19] C. D. Decker *et al.,* Phys. Plasmas **3**, 1360 (1996).
[20] E. Esarey *et al.,* Phys. Rev. Lett. **72**, 2887 (1994).
[21] N. E. Andreev *et al.,* Phys. Plasmas **2**, 2573 (1995).
[22] T. Katsouleas *et al.,* Part. Accel. **22**, 81 (1987).
[23] B. M. Penetrante and J. N. Bardsley, Phys. Rev. A **43**, 3100 (1991).
[24] S. C. Wilks *et al.,* Phys. Plasmas **2**, 264 (1995).
[25] Y. Kishimoto *et al.* (to be published).
[26] D. R. Nicholson, *Introduction to Plasma Theory* (Krieger, Malabar, Florida, 1992).